**REGULAR PAPER**

# Parametric Design Optimization of a Tail Mechanism Based on Tri-Wheels for Curved Spoke-Based Stair-Climbing Robots

JeongPil Shin[1] · YoungHwan Kim[1] · Dong-Yoon Kim[1] · Gil Ho Yoon[1] · TaeWon Seo[1]

## Abstract

Overcoming stairs is an important requirement for mobile robots. Therefore, many studies have been conducted to develop robots with novel stair-climbing mechanisms. A curved-spoke-based stair-climbing robot has been developed to overcome stairs, but had some limitations during stair climbing, such as damage caused by friction with the edge of the stair and impact during locomotion. In a previous study, several tail mechanisms were suggested to solve these problems, and the tri-wheel tail mechanism showed remarkable performance improvements. However, the previous study used only one step size of $300 \times 160$ mm$^2$. Therefore, in this study, a robust optimal design of the tri-wheel tail mechanism using the Taguchi method is conducted to achieve outstanding performance improvements even for stairs of various sizes and different climbing speeds as user conditions. The design of simulations of the tri-wheel tail mechanisms are performed via orthogonal arrays using a commercial dynamic simulation software tool. The objective function is to minimize the minimum required friction coefficient for a mobile robot to climb stairs without slip. The performance improvements are verified experimentally using a measurable performance index. Thus, these findings can be used to design stair-climbing mobile robots.

**Keywords** Tri-wheel · Tail mechanism · Stair-climbing · Mobile robot · Robust optimal design · Taguchi method

## 1 Introduction

Stairs are one of the most challenging obstacles for mobile robots to overcome. For a mobile robot to be useful, it must be able to climb stairs. Therefore, numerous robotic platforms have been studied with the aim to develop robots that can climb stairs without difficulty. ANYmal [1], a quadrupedal robot that features outstanding mobility and dynamic motion capability, can climb stairs reliably and quickly.

Legged robots, such as quadrupedal and bipedal robots, can navigate difficult terrain, such as small passageways or stairs, but they require sophisticated posture control and systems. Robots with simple mechanisms, such as wheels, tracks, and linkages, have been proposed to address the weaknesses of legged robots. The most typical mechanism for overcoming obstacles is a tracked robot, which requires a simple control system and design [2, 3]. Eccentric Crank Rover [4], a novel crank wheel mechanism with eccentric wheels and four-bar linkages, achieved high efficiency and mobility in rough terrain. In addition, curved-spoke-based stair-climbing robots have various mechanisms to overcome stair-climbing difficulties.

Numerous studies have been conducted on curved-spoke-based stair-climbing robots. Table 1 compares several curved-spoke-based stair-climbing robots. A curved-spoke tri-wheel (CSTW) mechanism [5], comprising a tri-wheel mechanism with curved spokes and a stopper mechanism, can climb stairs with noses or stairs without risers at a high speed. STEP [6], a mobile platform with 2-DOF transformable wheels, can overcome steps and stairs of various sizes that are typically encountered in indoor environments. RHex [7, 8], a hexapod with compliant legs and only six actuated

✉ TaeWon Seo
   taewonseo@hanyang.ac.kr

   JeongPil Shin
   jpshin9743@gmail.com

   YoungHwan Kim
   guma97@hanyang.ac.kr

   Dong-Yoon Kim
   roykim1011@gmail.com

   Gil Ho Yoon
   ghy@hanyang.ac.kr

1  Department of Mechanical Convergence Engineering, Hanyang University, 222, Wangsimni-ro, Seongdong-gu, Seoul 04763, Republic of Korea

**Table 1** Comparison of various curved-spoke-based stair-climbing robots

| Name | CSTW | RHex | STEP | LEVO |
|---|---|---|---|---|
| Picture |  |  |  |  |
| Mechanism | Curved-spoke tri-wheel | Hexapod with curved legs | 2-DOF transformable wheel | CSTW with switching primitives |
| Flat terrain mobility | − | + | −- | + |
| Stair-climbing stability | − | + | − | − |
| Design complexity | + | − | − | − |
| Characteristic | - Fast climbing speed | - Fast and seamless flat ground operation - Hexapod | - Shape-morphing wheel | - Wheel-mode switching - Flat ground operation |

degrees of freedom, has been developed to traverse highly fractured and unstable terrain as well as ascending and descending stairs. LEVO [9], a mobile robotic platform that uses wheel-mode switching primitives, has been proposed for stair climbing and high mobility on flat ground. Several studies have been performed with curved-spoke-based robots; however, the robots used in these have several drawbacks, such as impact during locomotion (CSTW, LEVO), damage and friction (resistance) problems owing to edge contact with stairs (CSTW, STEP, LEVO), demand for relatively many actuators (RHex), and complicated design (STEP, Tri-Wheel, LEVO). Because of these problems, the stability and climbing performance of curved-spoke-based stair-climbing robots is lessened.

In a previous study [10], several tail mechanisms, such as a curved linkage mechanism, tri-wheel mechanism, compliant mechanism with torsion spring and rotary damper, and compliant mechanism with translation spring, were proposed to overcome the limitations of curved-spoke-based stair-climbing robots. A comparative analysis of the tail mechanisms was performed through dynamic simulations based on various performance indices, linearity of the center of mass trajectory, RMS translational, and angular acceleration of the center of mass, friction requirements, and torque requirements. It was observed that the tail mechanisms improved the stability and stair-climbing performance of curved-spoke-based stair-climbing robots. The tri-wheel tail mechanism exhibited the most outstanding performance improvement.

Roboticists and biologists have been fascinated by tails for a long time. The tail is an essential and significant apparatus in organisms and climbing robots. Tails aid animals and robots in controlling their posture and increasing stability [11]. Climbing with a tail has advantages, such as the ability to grasp onto supports, maintain balance, and move from one location to another [12]. The gecko, a lizard with amazing arboreal acrobatic abilities, uses its tail as both a highly active control appendage and an emergency fifth leg to prevent falling during rapid climbing [13]. Similar to woodpeckers, treecreepers use their tails for support while climbing. This habit is related to structural adaptations other than climbing the trunk without tail support [14].

Many robotics researchers have studied tail mechanisms to manage the posture of robots and avoid unexpected tilting or falls. HELIOS Carrier [15], a tracked mobile platform with tail-like mechanism and control algorithm for stable motion in unknown environments, introduced a new simple tail-like mechanism to control the posture of the robot to avoid sudden tilting or falls. The simple and compact tail-like mechanism, consisting of a flexible rubber pipe attached to the rear of a basic tracked platform, permits the automatic motion support of the vehicle on steps and stairs by utilizing it to counteract the tilting behavior of the vehicle. The tail significantly improves the mobility of crawler robots while adding very little mass to the total mass of the robot. Tank-like module-based climbing robots [16, 17], an under-actuated modular climbing robot with flat dry elastomer adhesives, have been proposed to achieve high speed, high payload, and dexterous motions, which are typical drawbacks of previous climbing robots, using passive compliant joints and an active tail. The combination of the active tail and passive joints compensates for the pitch-back moment that causes the climbing robot to fall; furthermore, it creates a positive preload on the front wheel, which is essential for stable climbing of the tread mechanism. In addition, the compliance of the active tail helps the robot to perform external transitioning and overcome thin walls and obstacles without a complex controller.

In this study, a tri-wheel tail mechanism was analyzed and designed to maximize the performance improvement by applying the tri-wheel tail mechanism to solve the problems of curved-spoke-based stair-climbing robots. These problems include impact during locomotion and damage and friction problems due to edge contact with stairs [10]. Furthermore, while the previous study evaluated the performance improvement for a step size of $300 \times 160$ mm$^2$, this study proceeded with a robust optimal design using the Taguchi method [3, 18–22] of the tri-wheel tail mechanism to achieve excellent performance improvement even for stairs of various sizes. In this study, the CSTW platform was selected as one of several stair-climbing robot platforms that require the help of a tail and were used in the optimization of the tri-wheel tail mechanism. However, the tri-wheel tail mechanism optimized in this study is not limited in its application to the CSTW but is expected to show excellent effects for other stair-climbing robots that use tail assistance. This is because the CSTW mechanism was used as a driving unit for the tail mechanism in this study, but the tail mechanism can be used for other stair-climbing robot platforms. Therefore, the results of this study, which optimizes the tri-wheel tail mechanism, has versatile applicability in various robots. In addition, when applying the tri-wheel tail mechanism to other stair-climbing robot platforms, the results of the optimization analysis conducted in this study can be used as a reference to examine the effect of each design parameter of the tri-wheel tail mechanism on the performance.

A robust optimal design procedure was conducted using the Taguchi method [18], with the use of commercial dynamic simulation software, and design of simulations of the tri-wheel tail mechanism were performed using orthogonal arrays. In the simulation, the CSTW mechanism [5], which is the basic form of a curved-spoke-based stair-climbing robot, was used as a robotic platform. The objective function was to minimize the minimum required friction coefficient between the curved spoke wheel and the surface of the stairs. For the design parameter of the tri-wheel tail mechanism, four design parameters, namely, the linkage length $l_1$, radius length of the tri-wheel $l_2$, diameter of the tri-wheel $d_w$, and height of the fastening position of the tail mechanism to the body $h$, were adopted. The user conditions were stairs of various sizes and climbing speed of the robot. The S/N ratio was used to evaluate and optimize the tri-wheel tail mechanism. In addition, to experimentally verify the optimized results of the tri-wheel tail mechanism, actual stair-climbing experiments with the prototypes were conducted and the driving torque, a measurable performance indicator, was used. Therefore, the results of this study can be used to design stair-climbing robots.

The goal of this study is to optimize the shape of the tri-wheel tail mechanism to improve the climbing performance of the curved-spoke tri-wheel-based stair-climbing robot. The climbing performance of the curved-spoke tri-wheel-based stair-climbing robot is mainly determined by the slip occurrence by the friction between the stairs and the curved-spoke tri-wheel. As the minimum required friction coefficient acting between the curved-spoke tri-wheel and the stairs is lower, the robot can stably climb stairs even with low friction coefficient material. In the previous study of LEVO [9], it was found that the climbing capability of the LEVO was degraded when the payload applied to the robot increases. The impact during the locomotion and friction problem owing to contact with the nosing of the stairs cause slip of the CSTW of the robot during ascending. Slip occurrence indicates rise of the minimum required friction coefficient, so it degrades the performance. Therefore, in this study, it was determined that to minimize the minimum required friction coefficient, which had a great influence on the climbing performance of the robot, was set as the objective function.

The remainder of this study is organized as follows. Section 2 explains the curved-spoke-based stair-climbing robot and the importance of the tail mechanism along with a previous study on the design of the tail mechanism of a curved-spoke-based stair-climbing robot. Section 3 describes the optimal design procedure of the tri-wheel tail mechanism using the Taguchi method. Section 4 presents the experimental verification and results of the optimized tri-wheel tail mechanism. Section 5 presents the concluding remarks.

## 2 Description of Curved-Spoke Based Stair-Climbing Robot and Importance of Tail Mechanism

### 2.1 Description of Curved-Spoke Based Stair-Climbing Robot

In this study, the CSTW mechanism was selected as a curved spoke-based stair-climbing robot. For the robotic platform of the CSTW mechanism, LEVO [9] was utilized, which uses a normal wheel for driving on flat terrain and a CSTW for stair-climbing, as shown in Fig. 1. LEVO has two driving modes: a wheel mode using two in-wheel motors and two casters for driving on flat ground, and a CSTW mode using two curved-spoke tri-wheels (CSTW) and a tail for climbing stairs. The tail mechanism of LEVO is very simple; it consists of only a few aluminum frames that act as four-point supports as the robot climbs stairs.

Figure 2 shows the stair-climbing procedure used by LEVO. When the robot comes into contact with the stairs, the CSTW mode is activated, which causes the curved-spoke tri-wheels to be lowered and the rear caster to be raised. Consequently, the robot's curved-spoke tri-wheel
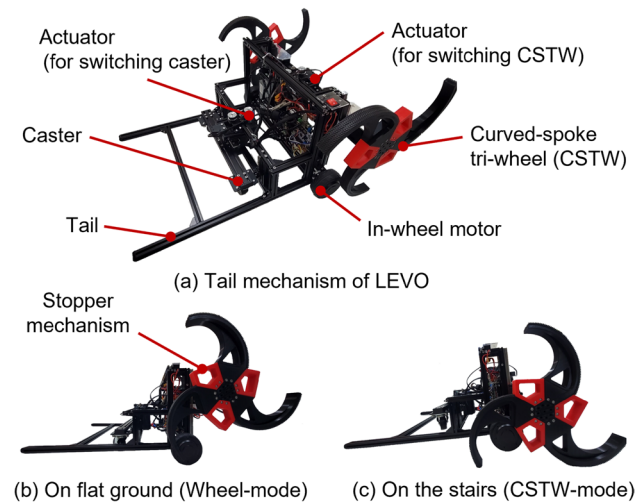
**Fig. 1** Mechanism configuration of the curved-spoke based stair-climbing robot (LEVO)
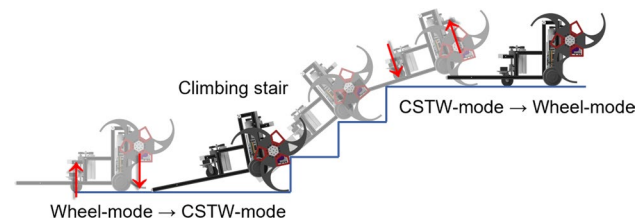


**Fig. 2** Stair-climbing process of LEVO

and tail make contact with the ground, and it climbs the steps by spinning its CSTW, with the tail providing four-point support.

The tail of LEVO has several shortcomings: damage and friction problems due to contact with the nosing and impact during climbing. The stability and stair-climbing performance of the robot suffer as a result; in particular, friction affects the stair-climbing ability of LEVO. Despite the existence of these problems, LEVO with its tail mechanism can climb stairs without slipping. However, this is feasible only if the coefficient of friction between the

nosing and tail mechanisms of LEVO is tiny. As the coefficient of friction increases, the stair-climbing performance is greatly reduced.

## 2.2 Importance of Tail Mechanism

In a previous study [10], a tri-wheel tail mechanism that is often adopted because it enables passive stair-climbing was proposed. The tri-wheel tail mechanism allows for stable stair-climbing while avoiding collisions and friction issues with the nosing. Because the mechanism has dual capacity of rolling and climbing, robots can climb stairs by rotating around the central axle of the tri-wheel tail mechanism and rolling along the surface of the stair until they reach a proper position to flip over and continue the climbing process [23]. As illustrated in Fig. 3a, a stair-climbing robot with a tri-wheel tail mechanism both climb stairs and maneuver on flat ground.

Shin [10] proposed several tail mechanisms for curved spoke-based stair-climbing robots. Tail mechanisms were created to enhance the stability and stair-climbing performance of curved-spoke-based stair-climbing robots and to solve the problems encountered by these robots when ascending stairs. The tail mechanisms were analyzed and compared using dynamic simulations based on various performance indices to assess performance improvement. Through a comparative analysis of the evaluation indices, the tri-wheel tail mechanism was confirmed to be the best among all the tail mechanisms proposed; additionally, it was found to be the most improved compared to the tail mechanism of LEVO. Consequently, using the tri-wheel tail mechanism improves the stair-climbing stability and performance of a curved-spoke-based stair-climbing robot and eliminates the difficulties that commonly impact stair climbing.

A robust optimal design process for the tri-wheel tail mechanism was conducted to maximize the performance improvement of the stair-climbing robot through the tri-wheel tail mechanism, which showed the best performance in a previous study, and to cope with stairs of various sizes. In the robust optimal design procedure, described in Sect. 3, the design of simulations were performed using a

**Fig. 3** Design parameters of the tri-wheel tail mechanism: on the flat ground, (b) on the stairs
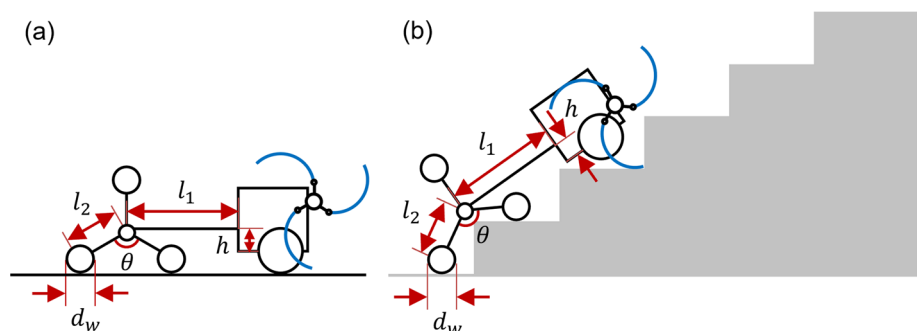
commercial dynamic simulation software tool, RecurDyn [24], instead of creating a dynamic simulation model by deriving kinematic or dynamic equations of the tri-wheel tail mechanism. The minimum required friction coefficient, which is the objective function in this study, cannot be obtained through the dynamic equation but can be obtained through static analysis. However, static analysis cannot find the minimum required friction coefficient by reflecting the climbing speed, which is the user condition considered in this study. Thus, in this study, optimization with the design of simulations was performed using a commercial dynamics simulation tool rather than optimization through mathematical analysis.

# 3 Robust Optimal Design Procedure with Taguchi Method

## 3.1 Optimal Design Problem

### 3.1.1 Taguchi Method and S/N Ratio

The Taguchi method is a systematic design methodology that uses the design of experiments or simulations to obtain an optimal value for each parameter [3, 19–22]. It is straightforward and cost-effective in establishing the objective function and satisfying several quality requirements simultaneously, as opposed to theoretical optimization approaches that often require complicated mathematical expansions. All principal factors that influence performance measures, such as signal-to-noise (S/N) ratio, can be categorized into two categories using this method: control factors and noise factors. A control factor is a process or product parameter that the design or production engineer can choose and control [19]. Noise factors are those that are expensive, challenging, or tough to manage during production or operation [19]. The control factors can be easily altered to desirable levels because they can be specified by a designer; however, the noise factors are difficult to control and result in variance or negative impact on product quality [3]. Thus, the control factors are the design parameters of the tri-wheel tail mechanism and the noise factors are the user conditions considered in this study.

In a robust design methodology, the S/N ratio is frequently used. The S/N ratio was introduced as a performance measure in the Taguchi method [19]. S/N ratio-based optimization improves the performance robustness of the system [25]. In addition, the mean and deviation can be considered simultaneously using the S/N ratio. The main purpose of optimization is to increase the S/N ratio because as the S/N ratio increases, the impact of random noise factors (the user conditions) on performance decreases. The objective function of this optimization was to minimize the minimum

required friction coefficient of the CSTW, so this optimization corresponded to the smaller-the-better case. Therefore, the following S/N ratio was adopted.

$$S/N = -10log_{10}|\frac{1}{N}\sum_{i=1}^{N}y_i^2|, \qquad (1)$$

where $N$ is the number of repetitions in the simulations and $y_i$ is the minimum required friction coefficient of the $i$-th simulation.

### 3.1.2 Objective Function

Friction and slip between the wheel and stairs are the most significant hurdles to stable stair climbing. If the frictional force acting between the wheel and stairs is smaller than the force generated by the driving torque of the wheel, the driving wheel tends to slip. This affects the performance of the driving wheel and the stair-climbing ability of the robot. The slip of the driving wheel is determined by variables such as the payload of the robot, geometric characteristics of the driving mechanism and road surface shape, and the materials of the wheel and stair surface, which are related to the friction coefficient and normal force exerted by the wheel on the stairs [26, 27].

The objective function of the optimization procedure was to minimize the minimum required friction coefficient between the curved-spoke wheel and the surface of stairs to enable the curved-spoke-based stair-climbing robot with the tri-wheel tail mechanism ascend stairs stably without slip. The minimum required friction coefficient is commonly used to assess stair-climbing stability [28]. Slipping occurs when the actual friction coefficient between the wheel and stair is less than the minimum required friction coefficient, and the robot is unable to ascend the stairs. The structural design can reduce the minimum required friction coefficient to obtain high stair-climbing capabilities. In this study, through iterative simulation, the minimum required friction coefficient of the CSTW was determined as the coefficient of friction when slipping did not occur in the CSTW to which the tri-wheel tail mechanism was applied.

### 3.1.3 Design Parameters and User Conditions

The design parameters of the tri-wheel tail mechanism used in this study are shown in Fig. 3, which are $l_1$, $l_2$, $d_w$, and $h$. $l_1$ and $l_2$ are the horizontal linkage length and radius of the tri-wheel, respectively; $d_w$ represents the diameter of the wheel and $h$ is the height of the fastening position of the tail mechanism to the body; and $\theta$ is a fixed parameter set to 120° to create a tri-wheel mechanism. Each design parameter is set to five different levels, and the values for each level are listed in Tables 2 and 5.

Stairs of various sizes (stair specification) and different climbing speeds were adopted as user conditions in the simulation. Each user condition was set at three levels, as can be seen in Tables 3 and 6. Various sizes of stairs were selected as a user condition because for the actual application of the stair-climbing mobile robot, it is necessary to be able to cope with stairs of different sizes. The values corresponding to each size of stairs were $260 \times 180$ mm$^2$, $300 \times 160$ mm$^2$, and $320 \times 100$ mm$^2$. Additionally, the climbing speed, defined as the number of steps that can be climbed per second [*step/s*], was adopted as a user condition. This is because the speed at which the stair-climbing mobile robot climbs stairs can vary depending on the target operating conditions. In the case of the curved-spoke-based stair-climbing robot, because the climbing speed is determined according to the rotation speed of the CSTW, the CSTW rotation speed [*rpm*] was used as a variable to represent the climbing speed. The values for each level of climbing speed were 0.5 *step/s* (10 *rpm*), 1.0 *step/s* (20 *rpm*), and 1.5 *step/s* (30 *rpm*).

## 3.2 Design of Simulations Using Orthogonal Arrays

### 3.2.1 Simulation Environment

Simulations of the tri-wheel tail mechanism were designed using orthogonal arrays (OA). Stair-climbing simulations of the tri-wheel tail mechanism were conducted to determine the minimum required friction coefficient by using a commercial dynamic simulation software tool, RecurDyn. The minimum required friction coefficient of the CSTW was determined to be the friction coefficient when slipping does not occur in the CSTW and the surface of the stairs through an iterative simulation process in the dynamic simulation. The simulations when the minimum required friction coefficient was obtained indicates the situation just before the slip occurs.

A simplified 3D model of the tri-wheel tail mechanism was used for the simulation. Each model consisted of two CSTWs at the front and a tri-wheel tail mechanism. As shown in Fig. 4, a simplified 3D model of the curved-spoke based stair-climbing robot with the tri-wheel tail mechanism

climbed stairs of various sizes at different climbing speeds. The rotating speed of the CSTW, which determines the climbing speed, was used as control input in the simulation. The CSTW of the model was designed to fit the selected stair sizes. Lee [29] determined an optimized shape that enables the CSTW mechanism to stably and smoothly climb stairs of three different sizes: $260 \times 180$ mm$^2$, $300 \times 160$ mm$^2$, and $320 \times 100$ mm$^2$. As can be seen in Fig. 5, the optimal values of the design parameters of the CSTW were $R_1 = 96$ mm, $\theta_1 = 52°$, $R_2 = 139$ mm, and $\theta_2 = 118°$. These optimal values were used to design the CSTW used in the simulation.

To determine the minimum required friction coefficient for stable stair-climbing without slipping, the dynamic friction coefficient between the CSTW and stair surface was set from high (1.0, non-slip) to low. The friction coefficient between the wheel of the tri-wheel tail mechanism and stair surface was assumed to be 1.0, which is a non-slip condition. In the case of the tail mechanism of LEVO, without the tri-wheel tail mechanism, friction occurred between the nosing of the stairs and tail mechanism when the robot climbed the stairs. At this time, the coefficient of friction between the nosing of the stairs and tail mechanism was assumed to be 0.1. For the simulation, it was critical to establish contact
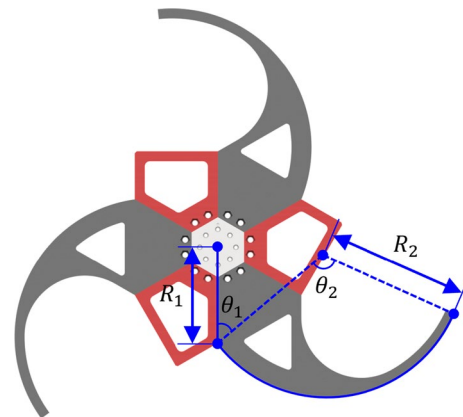
**Fig. 5** Four design parameters of the CSTW. Based on the previous literature [29], the optimal CSTW design parameter values for stairs of various sizes were used in the simulation

**Fig. 4** Simulation environment. A curved-spoke based stair-climbing robot with the tri-wheel tail mechanism climbed stairs of various sizes at multiple climbing speeds
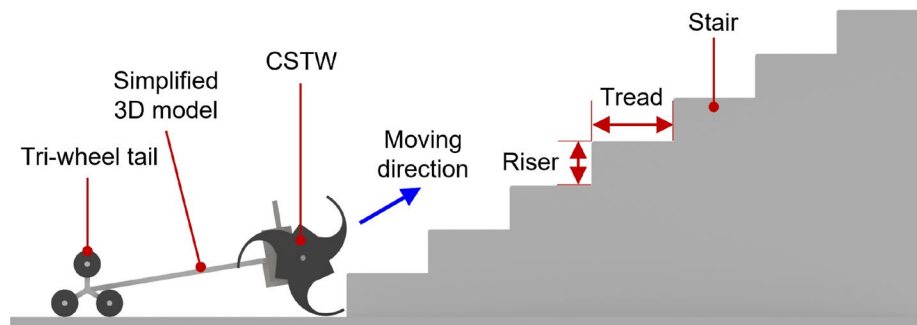
**Table 2** Levels of design parameters for the first simulation

| Design parameter | Level 1 | Level 2 | Level 3 | Level 4 | Level 5 |
|---|---|---|---|---|---|
| $l_1$ [mm] | 450 | 500 | 550 | 600 | 650 |
| $l_2$ [mm] | 90 | 100 | 110 | 120 | 130 |
| $d_w$ [mm] | 80 | 90 | 100 | 110 | 120 |
| $h$ [mm] | 20 | 40 | 60 | 80 | 100 |

**Table 3** Levels of user conditions for the first simulation

| User condition | Level 1 | Level 2 | Level 3 |
|---|---|---|---|
| Stair specification (Tread × Riser) [mm$^2$] | 260 × 180 | 300 × 160 | 320 × 100 |
| Climbing speed [step/s] (RPM of CSTW [rpm]) | 0.5 (10) | 1.0 (20) | 1.5 (30) |

conditions between the CSTW and stair surface as well as between the tri-wheel tail mechanism and stair surface. The stiffness and damping coefficients for the contact conditions were set to 100000 N/mm and 10 N/$mm \cdot s$, respectively. The simulation time were 14 s (0.5 *step/s*), 7 s (1.0 *step/s*), and 4.7 s (1.5 *step/s*); and the number of steps were 1000. The maximum time step, which was the upper-bound time-step size of the integrator during dynamic analysis, was 1.e-002.

### 3.2.2 First Simulation Results

In the design of simulations using the OAs, the stair-climbing performance and sensitivity were analyzed based on the minimum required friction coefficient and S/N ratio according to each design parameter and user condition. In Sect. 3.2, two optimization simulations were performed: the first simulation in Sect. 3.2.2 and second simulation in Sect. 3.2.3. The design parameters and user conditions used for the first simulation are listed in Tables 2 and 3, respectively.

Table 4 presents the results of the first simulation. For each simulation from the orthogonal array $L_{25}(5^4)$, the resulting objective function and S/N ratio are summarized in Table 4. In Table 4, there are blanks for the objective function value for each user condition level, which represent contact or collision between the tri-wheel tail mechanism and the nosing of the stairs during the stair-climbing simulation. When calculating the S/N ratio, the value of the objective function in the blank was assumed to be 1.0. To examine the underlying effects of various design parameters on the objective function, S/N ratios were calculated for each design parameter at different levels, as shown in Fig. 6. It can be observed in Fig. 6 that the design parameter $l_1$, $l_2$, and $d_w$ of level 5, 2, and 3, respectively, are optimal as the

corresponding S/N ratio is maximized for those levels of design parameters. This is further confirmed by the data presented in Table 4. In the case of the design parameter $h$, $h$ exhibited the largest S/N ratio at level 5, but it was determined that it had an optimal value at level 2 rather than level 5. This is because $h$ is the height of the fastening position and the position of the center of mass of the robot increases as the value increases. This adversely affects the reduction in the friction coefficient value, which is the objective function.

### 3.2.3 Second Simulation Results

Based on the results of the first simulation, the second simulation was performed. In the first simulation, it was determined that $d_w$ at level 3 was the optimal value. The optimization procedures were subsequently repeated to search for more accurate optimal values by appropriately adopting another reduced orthogonal array with the design parameters $l_1$, $l_2$, and $h$. In the second simulation, the user condition of climbing speed was used at two levels rather than three levels. This is because the sensitivity analysis via the S/N ratio of the climbing speed in the first simulation showed that level 2 of the climbing speed (1.0 *step/s* (20 *rpm*)) was not sensitive. Tables 5 and 6 indicate the design parameters and user conditions used in the second simulation, respectively.

The results of the second simulation are shown in Table 7. Table 7 summarizes the resulting objective function and S/N ratio for each simulation from the orthogonal array $L_{25}(5^3)$. As can be seen in Fig. 7, the S/N ratios are calculated for $l_1$, $l_2$ and $h$ at different levels. According to the S/N ratios of the second simulation, the optimal levels for $l_1$, $l_2$ and $h$ were 5, 2, and 3, respectively. Therefore, the optimal values for the design parameters of the tri-wheel tail mechanism are $l_1 = 670$ mm, $l_2 = 95$ mm, $d_w = 100$ mm, and $h = 100$ mm. These optimal design parameter values allow the tri-wheel tail mechanism to secure outstanding performance improvements, even for stairs of various sizes and different climbing speeds.

The results of comparing the S/N ratios of the first and second simulations are shown in Fig. 8. The S/N ratios of the second simulation are significantly improved by more than 1.08 *dB* as compared to those in the first simulation. Figure 9 indicates the S/N ratios calculated for the user conditions (stair specification and climbing speed) in the first

**Table 4** Resulting objective functions and S/N ratios of $L_{25}(5^4)$ orthogonal array for the first simulation (C.S.: Climbing speed)

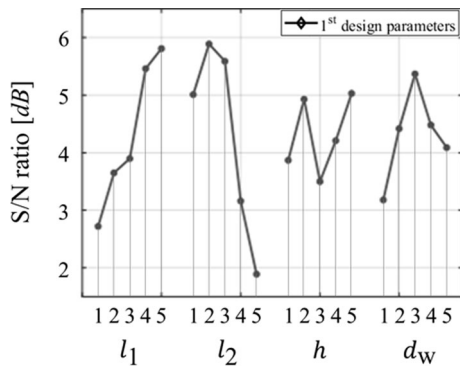| No. | Design parameter | | | | Objective function (minimum required friction coefficient) | | | | | | | | | S/N ratio [dB] |
|---|---|---|---|---|---|---|---|---|---|---|---|---|---|---|
| | $l_1$ (Level) | $l_2$ (Level) | $d_w$ (Level) | $h$ (Level) | Stair specification 1 | | | Stair specification 2 | | | Stair specification 3 | | | |
| | | | | | C.S. 1 | C.S. 2 | C.S. 3 | C.S. 1 | C.S. 2 | C.S. 3 | C.S. 1 | C.S. 2 | C.S. 3 | |
| 1 | 1 | 1 | 1 | 1 | – | – | – | – | – | 0.57 | 0.58 | 0.54 | 0.59 | 1.55 |
| 2 | 1 | 2 | 2 | 2 | 0.42 | 0.46 | 0.51 | 0.41 | 0.44 | 0.54 | 0.74 | 0.80 | 0.92 | 4.31 |
| 3 | 1 | 3 | 3 | 3 | 0.43 | 0.45 | 0.49 | 0.47 | 0.49 | 0.58 | 0.77 | 0.70 | 0.82 | 4.52 |
| 4 | 1 | 4 | 4 | 4 | – | – | – | 0.54 | 0.56 | 0.62 | 0.74 | 0.75 | 0.94 | 1.77 |
| 5 | 1 | 5 | 5 | 5 | – | – | – | 0.57 | 0.59 | 0.70 | 0.82 | 0.86 | 0.93 | 1.45 |
| 6 | 2 | 1 | 2 | 3 | 0.54 | 0.57 | 0.58 | 0.53 | 0.55 | 0.61 | 0.73 | 0.74 | 0.78 | 3.98 |
| 7 | 2 | 2 | 3 | 4 | 0.40 | 0.42 | 0.52 | 0.33 | 0.31 | 0.40 | 0.58 | 0.62 | 0.65 | 6.29 |
| 8 | 2 | 3 | 4 | 5 | 0.46 | 0.47 | 0.57 | 0.48 | 0.49 | 0.54 | 0.70 | 0.73 | 0.75 | 4.62 |
| 9 | 2 | 4 | 5 | 1 | – | – | – | 0.53 | 0.54 | 0.57 | 0.76 | 0.77 | 0.80 | 1.98 |
| 10 | 2 | 5 | 1 | 2 | 0.41 | 0.42 | 0.46 | – | – | – | – | – | – | 1.38 |
| 11 | 3 | 1 | 3 | 5 | 0.36 | 0.37 | 0.39 | 0.42 | 0.44 | 0.47 | 0.51 | 0.52 | 0.55 | 6.89 |
| 12 | 3 | 2 | 4 | 1 | 0.39 | 0.41 | 0.43 | 0.43 | 0.48 | 0.52 | 0.54 | 0.58 | 0.63 | 6.09 |
| 13 | 3 | 3 | 5 | 2 | 0.43 | 0.45 | 0.49 | 0.48 | 0.52 | 0.53 | 0.60 | 0.62 | 0.68 | 5.37 |
| 14 | 3 | 4 | 1 | 3 | – | – | – | – | – | – | – | – | – | 0.00 |
| 15 | 3 | 5 | 2 | 4 | – | – | – | – | – | – | 0.52 | 0.52 | 0.60 | 1.15 |
| 16 | 4 | 1 | 4 | 2 | 0.41 | 0.42 | 0.48 | 0.39 | 0.43 | 0.49 | 0.45 | 0.34 | 0.57 | 7.00 |
| 17 | 4 | 2 | 5 | 3 | 0.40 | 0.41 | 0.48 | 0.43 | 0.46 | 0.52 | 0.52 | 0.56 | 0.65 | 6.06 |
| 18 | 4 | 3 | 1 | 4 | 0.35 | 0.32 | 0.58 | 0.36 | 0.37 | 0.42 | 0.56 | 0.63 | 0.65 | 6.24 |
| 19 | 4 | 4 | 2 | 5 | 0.31 | 0.48 | 0.59 | 0.41 | 0.42 | 0.45 | 0.59 | 0.70 | 0.71 | 5.45 |
| 20 | 4 | 5 | 3 | 1 | – | – | – | 0.43 | 0.46 | 0.52 | 0.61 | 0.68 | 0.72 | 2.54 |
| 21 | 5 | 1 | 5 | 4 | 0.46 | 0.45 | 0.50 | 0.45 | 0.46 | 0.48 | 0.61 | 0.62 | 0.64 | 5.61 |
| 22 | 5 | 2 | 1 | 5 | 0.33 | 0.34 | 0.42 | 0.35 | 0.36 | 0.37 | 0.59 | 0.60 | 0.65 | 6.71 |
| 23 | 5 | 3 | 2 | 1 | 0.35 | 0.36 | 0.41 | 0.37 | 0.40 | 0.44 | 0.5 | 0.51 | 0.54 | 7.21 |
| 24 | 5 | 4 | 3 | 2 | 0.43 | 0.44 | 0.47 | 0.41 | 0.42 | 0.44 | 0.51 | 0.52 | 0.55 | 6.60 |
| 25 | 5 | 5 | 4 | 3 | – | – | – | 0.44 | 0.45 | 0.51 | 0.53 | 0.54 | 0.59 | 2.94 |



**Fig. 6** S/N ratio for the design parameters in the first simulation

and second simulations. The S/N ratios are greater for level 1 of the stair specification, which is a high-slope stair, and for level 1 of the climbing speed, which is a low climbing speed.

To evaluate the performance improvements, the objective function (minimum required friction coefficient) between the model without the tail mechanism, the initial tri-wheel tail mechanism, and the optimized tri-wheel tail mechanism were compared in Table 8. Figure 10 depicts the three tail mechanisms analyzed in Table 8. Compared with the model without the tri-wheel tail mechanism, the initial tri-wheel tail mechanism exhibited an average decrease of 17.8% in the minimum required friction coefficient, whereas the optimized tri-wheel tail mechanism exhibited an average decrease of 32.0% in the minimum required friction coefficient.

## 4 Experimental Verification and Results

The optimization results of Sect. 3.2 were based on the simulations. Next, experimental verification through actual stair-climbing experiments using the tri-wheel tail mechanism was performed. To verify the performance improvements, the minimum required friction coefficient, which was the objective function value, should be measured. However, it is

**Table 5** Levels of design parameters for the second simulation

| Design parameter | Level 1 | Level 2 | Level 3 | Level 4 | Level 5 |
|---|---|---|---|---|---|
| $l_1$ [mm] | 630 | 640 | 650 | 660 | 670 |
| $l_2$ [mm] | 90 | 95 | 100 | 105 | 110 |
| $h$ [mm] | 90 | 95 | 100 | 105 | 110 |

**Table 6** Levels of user conditions for the second simulation

| User condition | Level 1 | Level 2 | Level 3 |
|---|---|---|---|
| Stair specification (Tread × Riser) [mm²] | 260 × 180 | 300 × 160 | 320 × 100 |
| Climbing speed [step/s] (RPM of CSTW [rpm]) | 0.5 (10) | 1.5 (30) | |

not easy to measure the coefficient of friction of the CSTW in practice. Hence, the driving torque of the motor of the CSTW was measured instead. Thus, improvement in the friction coefficient could be substantiated through the relationship between the driving torque and coefficient of friction of the CSTW derived in the static analysis. Therefore, the driving torque in the actual experiments and simulations of the model without the tri-wheel tail mechanism, the initial tri-wheel tail mechanism, and the optimized tri-wheel tail mechanism were analyzed and compared.

**Table 7** Resulting objective functions and S/N ratios of $L_{25}(5^3)$ orthogonal array for the second simulation (C.S.: Climbing speed)

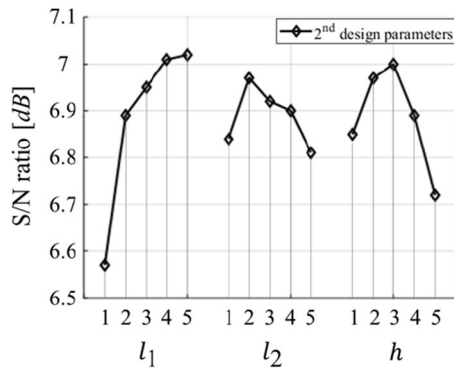| No. | Design parameter | | | Objective function (minimum required friction coefficient) | | | | | | S/N ratio [dB] |
|---|---|---|---|---|---|---|---|---|---|---|
| | $l_1$ (Level) | $l_2$ (Level) | $h$ (Level) | Stair specification 1 | | Stair specification 2 | | Stair specification 3 | | |
| | | | | C.S. 1 | C.S. 2 | C.S. 1 | C.S. 2 | C.S. 1 | C.S. 2 | |
| 1 | 1 | 1 | 1 | 0.43 | 0.45 | 0.38 | 0.51 | 0.52 | 0.58 | 6.32 |
| 2 | 1 | 2 | 2 | 0.38 | 0.46 | 0.39 | 0.44 | 0.55 | 0.58 | 6.51 |
| 3 | 1 | 3 | 3 | 0.35 | 0.41 | 0.40 | 0.43 | 0.53 | 0.56 | 6.88 |
| 4 | 1 | 4 | 4 | 0.36 | 0.44 | 0.39 | 0.43 | 0.54 | 0.57 | 6.72 |
| 5 | 1 | 5 | 5 | 0.38 | 0.46 | 0.40 | 0.47 | 0.54 | 0.59 | 6.39 |
| 6 | 2 | 1 | 2 | 0.41 | 0.47 | 0.37 | 0.46 | 0.44 | 0.57 | 6.79 |
| 7 | 2 | 2 | 3 | 0.37 | 0.44 | 0.36 | 0.43 | 0.46 | 0.51 | 7.30 |
| 8 | 2 | 3 | 4 | 0.37 | 0.46 | 0.38 | 0.43 | 0.52 | 0.58 | 6.69 |
| 9 | 2 | 4 | 5 | 0.36 | 0.44 | 0.40 | 0.44 | 0.51 | 0.56 | 6.81 |
| 10 | 2 | 5 | 1 | 0.38 | 0.41 | 0.39 | 0.44 | 0.50 | 0.57 | 6.87 |
| 11 | 3 | 1 | 3 | 0.37 | 0.44 | 0.34 | 0.40 | 0.50 | 0.54 | 7.18 |
| 12 | 3 | 2 | 4 | 0.36 | 0.43 | 0.35 | 0.42 | 0.50 | 0.57 | 7.03 |
| 13 | 3 | 3 | 5 | 0.40 | 0.47 | 0.38 | 0.40 | 0.52 | 0.58 | 6.67 |
| 14 | 3 | 4 | 1 | 0.37 | 0.45 | 0.35 | 0.41 | 0.51 | 0.56 | 6.98 |
| 15 | 3 | 5 | 2 | 0.36 | 0.44 | 0.39 | 0.46 | 0.49 | 0.55 | 6.88 |
| 16 | 4 | 1 | 4 | 0.41 | 0.46 | 0.37 | 0.44 | 0.47 | 0.51 | 7.02 |
| 17 | 4 | 2 | 5 | 0.36 | 0.43 | 0.38 | 0.45 | 0.51 | 0.56 | 6.86 |
| 18 | 4 | 3 | 1 | 0.35 | 0.44 | 0.38 | 0.44 | 0.49 | 0.56 | 6.96 |
| 19 | 4 | 4 | 2 | 0.34 | 0.42 | 0.37 | 0.46 | 0.47 | 0.51 | 7.28 |
| 20 | 4 | 5 | 3 | 0.36 | 0.40 | 0.40 | 0.45 | 0.50 | 0.56 | 6.93 |
| 21 | 5 | 1 | 5 | 0.40 | 0.47 | 0.37 | 0.47 | 0.48 | 0.51 | 6.89 |
| 22 | 5 | 2 | 1 | 0.36 | 0.46 | 0.38 | 0.45 | 0.47 | 0.50 | 7.14 |
| 23 | 5 | 3 | 2 | 0.34 | 0.40 | 0.37 | 0.44 | 0.48 | 0.51 | 7.38 |
| 24 | 5 | 4 | 3 | 0.40 | 0.52 | 0.37 | 0.43 | 0.49 | 0.54 | 6.70 |
| 25 | 5 | 5 | 4 | 0.37 | 0.45 | 0.40 | 0.46 | 0.47 | 0.52 | 6.98 |

Fig. 7 S/N ratio for the design parameters in the second simulation
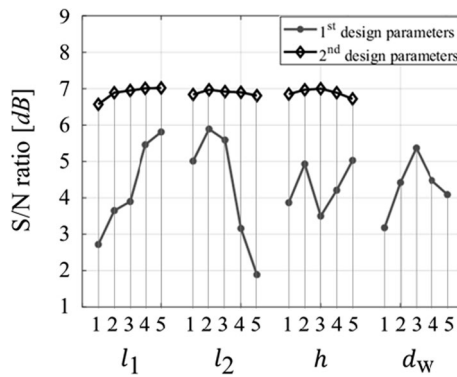


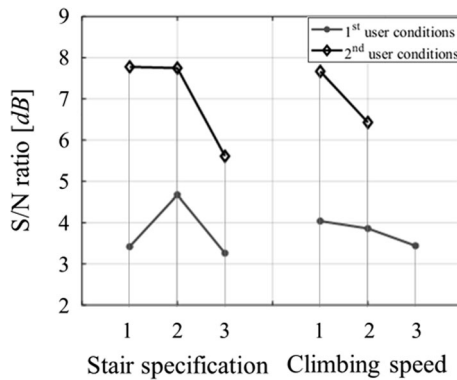Fig. 8 S/N ratio for the design parameters in the first and second simulations



Fig. 9 S/N ratio for the user conditions in the first and second simulation

## 4.1 Static Analysis of the CSTW

Static analysis of the CSTW was performed based on the free-body diagram shown in Fig. 11 to determine the relationship between the driving torque ($\tau$) and coefficient of friction ($\mu_1$) of the CSTW. Herein, $\mu_1$ is the friction coefficient between

Table 8 Comparison results of the objective function (minimum required friction coefficient) between the model without tail mechanism, the initial tri-wheel tail mechanism, and the optimized tri-wheel tail mechanism (C.S.: Climbing speed)

| No. | Tail mechanism | Design parameter | | | | Objective function (minimum required friction coefficient) | | | | | | | | | S/N ratio [dB] |
|---|---|---|---|---|---|---|---|---|---|---|---|---|---|---|---|
| | | $l_1$ [mm] | $l_2$ [mm] | $d_w$ [mm] | $h$ [mm] | Stair specification 1 | | | Stair specification 2 | | | Stair specification 3 | | | |
| | | | | | | C.S. 1 | C.S. 2 | C.S. 3 | C.S. 1 | C.S. 2 | C.S. 3 | C.S. 1 | C.S. 2 | C.S. 3 | |
| 1 | Without tail | 550 | – | | | 0.58 | 0.57 | 0.67 | 0.55 | 0.58 | 0.65 | 0.42 | 0.65 | 0.75 | 4.31 |
| 2 | Initial tri-wheel tail | 550 | 110 | 100 | 60 | 0.40 | 0.43 | 0.48 | 0.44 | 0.47 | 0.55 | 0.56 | 0.58 | 0.64 | 5.83 |
| 3 | Opt. tri-wheel tail | 670 | 95 | 100 | 100 | 0.35 | 0.36 | 0.43 | 0.33 | 0.34 | 0.40 | 0.45 | 0.46 | 0.50 | 7.82 |
| | 1–2 Decrement [%] | | | | | 31.0 | 24.6 | 28.4 | 20.0 | 19.0 | 15.4 | -3.3 | 10.8 | 14.7 | |
| | 1–3 Decrement [%] | | | | | 39.7 | 36.8 | 35.8 | 40.0 | 41.4 | 38.5 | -7.1 | 29.2 | 33.3 | |
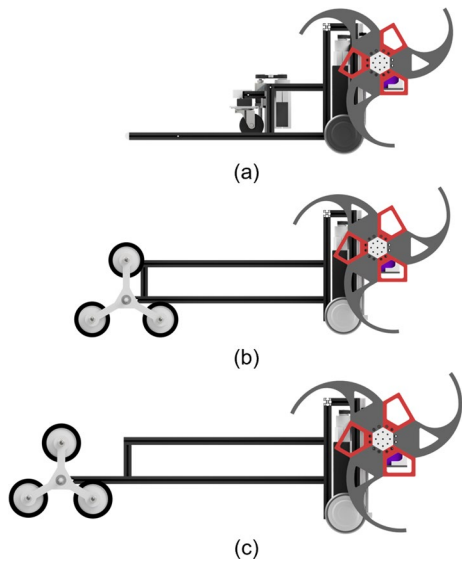
**Fig. 10** Rendering of the three tail mechanisms: **a** Without the tri-wheel tail mechanism; **b** Initial tri-wheel tail mechanism; **c** Optimized tri-wheel tail mechanism
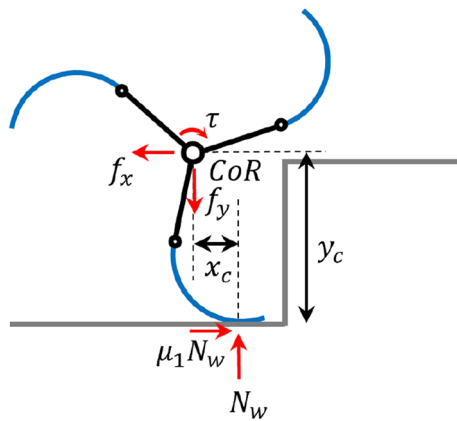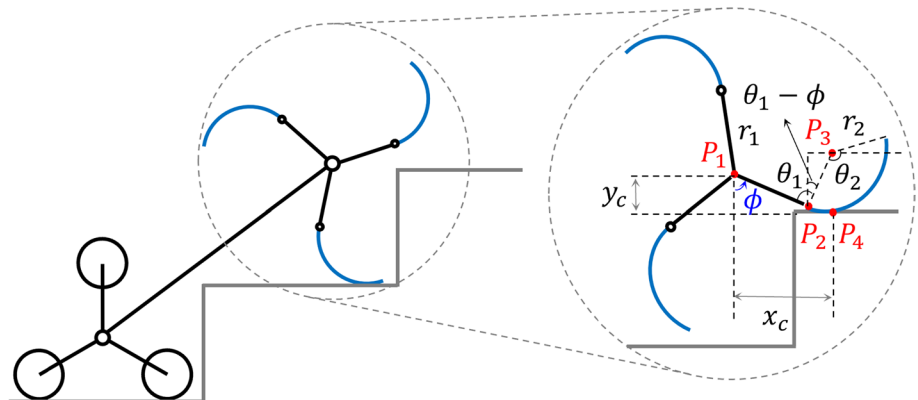
the CSTW and the surface of the stairs; $\tau$ denotes the driving torque at the center of rotation (CoR); $N_w$ denotes the normal force at the contact point of the CSTW; $f_x$ and $f_y$ denote the reaction forces at the CoR; and $x_c$ and $y_c$ are the distances between the contact point of the spoke and the CoR during stair climbing. The force equilibrium Eqs. 2)–(4) for the CSTW while climbing stairs [5] are as follows.

$$\Sigma F_x = \mu_1 N_w - f_x = 0, \tag{2}$$

$$\Sigma F_y = -N_w + f_y = 0, \tag{3}$$

$$\Sigma M_{CoR} = -N_w x_c - \mu_1 N_w y_c + \tau = 0. \tag{4}$$

Based on the Eqs. (2)–(4), the relationship between the driving torque ($\tau$) and the coefficient of friction ($\mu_1$) of the CSTW can be derived as follows. Here, $\mu_1$ represents the static coefficient of friction.

$$\therefore \mu_1 \geq \frac{\tau - N_w x_c}{N_w y_c}. \tag{5}$$

$x_c$ and $y_c$ can be defined based on the kinematics of the CSTW during stair-climbing [9] shown in Fig. 12. Herein, $\phi$ and $\theta_1$ represent the input angle of CSTW and the initial value of $\phi$, respectively. The point displacements of CSTW are denoted as $P_1$, $P_2$, $P_3$, and $P_4$. Assuming that the nosing of the stairs is the origin, $P_1$, $P_2$, $P_3$, and $P_4$ can be determined as follows.

$$P_1 = \begin{bmatrix} r_2\{\theta_1 - \phi - \sin(\theta_1 - \phi)\} - r_1 \sin\phi \\ r_2\{1 - \cos(\theta_1 - \phi)\} + r_1 \cos\phi \end{bmatrix}, \tag{6}$$

$$P_2 = r_2 \begin{bmatrix} \theta_1 - \phi - \sin(\theta_1 - \phi) \\ 1 - \cos(\theta_1 - \phi) \end{bmatrix}, \tag{7}$$



**Fig. 11** Free-body diagram of the CSTW during stair-climbing

**Fig. 12** Kinematic analysis of the CSTW mechanism with the tri-wheel tail mechanism during stair-climbing

$$P_3 = r_2 \begin{bmatrix} \theta_1 - \phi \\ 1 \end{bmatrix}, \tag{8}$$

$$P_4 = r_2 \begin{bmatrix} \theta_1 - \phi \\ 0 \end{bmatrix}. \tag{9}$$

Using the Eqs. (6)–(9), $x_c$ and $y_c$ can be derived as follows:

$$x_c = P_{4_x} - P_{1_X}, \quad y_c = P_{1_y}. \tag{10}$$

According to the simulation result and Inequal. (5), it was found that the friction coefficient tends to increase as the driving torque increases. In this simulation, constant CSTW rotational speeds of 10, 20, and 30 *rpm* were set to be maintained, and the driving torque acting on the CSTW to maintain the rotational speed was obtained from the simulation data. In a situation where the friction coefficient is fixed, the CSTW system can operate without slipping even if a smaller driving torque is applied according to Inequal. (5). However, the driving torque obtained in this simulation is the driving torque required to maintain the corresponding rotational speed. Thus, in this study, it was considered that the proportional relationship between these two parameters, the friction coefficient and the driving torque, is established, and it was tried to see the change in the friction coefficient indirectly by measuring the driving torque that can be measured since it is difficult to actually measure the friction coefficient used as the objective function.

## 4.2 Prototype Robot and Experiment Condition

Three prototypes—a model without the tri-wheel tail mechanism, an initial tri-wheel tail mechanism, and an optimized tri-wheel tail mechanism—were designed and created for experimental verification. Figure 13 shows the three prototypes used in the stair-climbing experiments. These prototypes were constructed based on the design parameters ($l_1$, $l_2$, $d_w$, and $h$), as described in Table 8. The dimensions of the three prototypes use the values of each of the aforementioned design parameters, and the width in all cases is 700 mm.

As shown in Fig. 5, the CSTW was manufactured by 3D printing using the optimal CSTW design parameter values discussed in Sect. 3.2.1. For the driving motor of the CSTW, servo motors (PH54-200-S500-R, ROBOTIS), including the encoder and controller, were used. The main body and tri-wheel tail mechanism were composed of aluminum frames. The spokes of the tri-wheel tail mechanism were fabricated by cutting acrylic plates using a laser cutter according to design parameter $l_2$. The wheels of the tri-wheel tail mechanism were commercial wheels of a size that fit the value of the design parameter $d_w$.

As can be seen in Fig. 14, stairs of $300 \times 160$ mm$^2$, which is one of the user conditions for stair size, were utilized for the stair-climbing experiments of the prototypes. In the stair-climbing experiments, the rotation speed of the CSTW was set to 10 *rpm*; thus, the climbing speed, which is one of the user conditions, was 0.5 *step/s*.

**Fig. 13** Prototype robots for the experiment: **a** Without the tri-wheel tail mechanism, **b** Initial tri-wheel tail mechanism, **c** Optimized tri-wheel tail mechanism
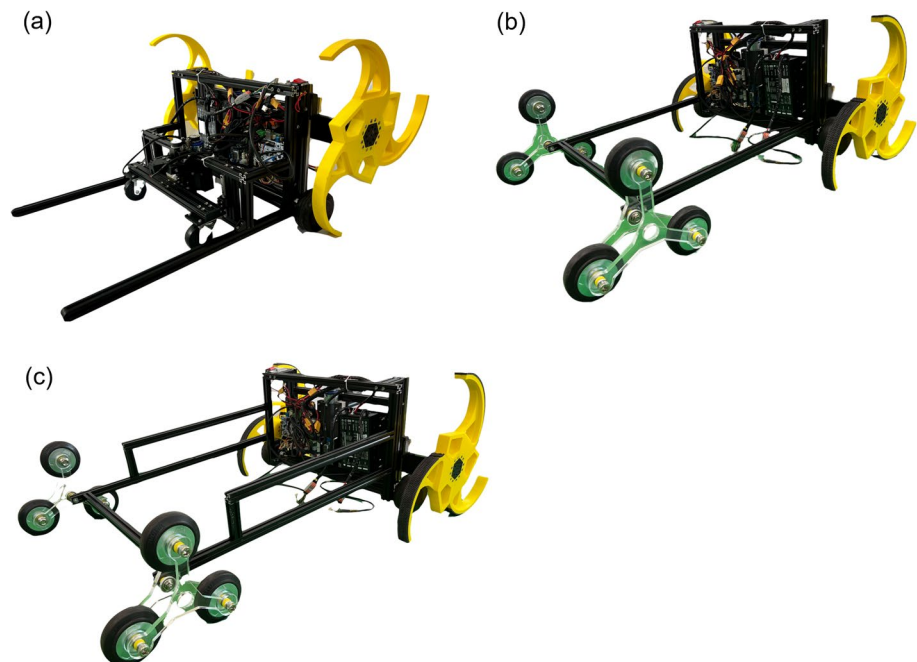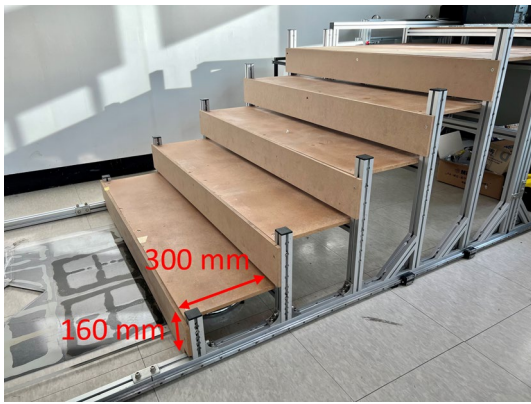
**Fig. 14** Test-bed used in the stair-climbing experiment: Stairs of 300 × 160mm²

### 4.3 Experimental Results

As shown in Fig. 15, stair-climbing experiments using the three different tail mechanisms were performed. During the experiments, the driving torque of the motor of the CSTW of each prototype was measured and analyzed to validate the performance improvement of the minimum required friction coefficient of the CSTW.

The required torque of the motor for steady stair-climbing was estimated using the driving torque. Typically, the required torque is determined by utilizing the peak torque value [26, 27]. In contrast, the peak torque value of the driving torque occurred when the CSTW stopper came in contact with the nosing in the CSTW mechanism. Therefore, the influence of the tri-wheel tail mechanism on the peak torque value was limited [10]. Thus, the RMS value of the driving

torque was used to measure and evaluate the overall influence of the tri-wheel tail mechanism on the driving torque. The RMS driving torque was calculated based on the measured driving torque of the motor during stair climbing and was derived as follows.

$$T_{RMS} = \sqrt{\frac{1}{N} \sum_{i=1}^{N} (T_i)^2}, \tag{11}$$

where $T_i$ is the driving torque of the $i$-th step in the simulation and the $i$-th measured driving torque data in the actual experiment, $N$ is the total number of steps in the simulation and the total number of data points in the actual experiment.

Table 9 and Fig. 16 summarizes the comparison results of the RMS driving torque between the model without the tri-wheel tail mechanism, the initial tri-wheel tail mechanism,

**Table 9** Comparison results of the RMS driving torque between the model without the tri-wheel tail mechanism, the initial tri-wheel tail mechanism, and the optimized tri-wheel tail mechanism in the experiments and the simulations

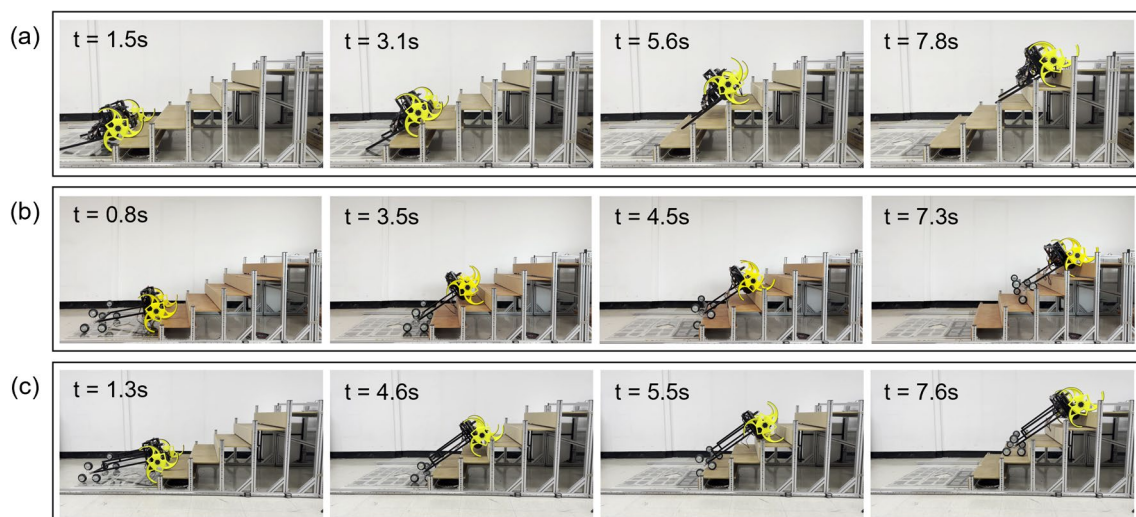| No. | Tail mechanism | RMS driving torque [$N \cdot m$] | |
|-----|----------------|------------|------------|
| | | Simulation | Experiment |
| 1 | Without tail | 25.71 | 36.32 |
| 2 | Initial tri-wheel tail | 23.01 | 31.70 |
| 3 | Optimized tri-wheel tail | 21.34 | 29.91 |
| 1-2 Decrement [%] | | 10.5 | 12.7 |
| 1-3 Decrement [%] | | 17.0 | 17.6 |



**Fig. 15** Experimental results of three different tail mechanisms (Experimental video can be found in the Additional file 1): **a** Without the tri-wheel tail mechanism, **b** Initial tri-wheel tail mechanism, **c** Optimized tri-wheel tail mechanism
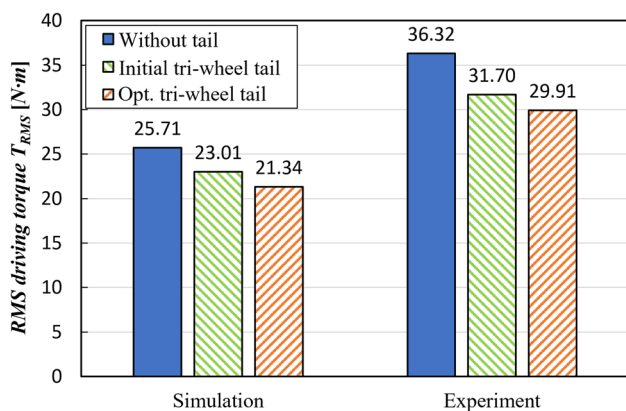
**Fig. 16** The RMS driving torque of the model without the tri-wheel tail mechanism, the initial tri-wheel tail mechanism, and the optimized tri-wheel tail mechanism in the experiments and the simulations

and the optimized tri-wheel tail mechanism obtained through experiments and simulations. In the simulations, compared with the model without the tri-wheel tail mechanism, the initial tri-wheel tail mechanism showed a decrease of 10.5% in the RMS driving torque, whereas the optimized tri-wheel tail mechanism showed a decrease of 17.0% in the RMS driving torque. In the actual experiments, compared to the model without the tri-wheel tail mechanism, the RMS driving torque of the initial tri-wheel tail mechanism was reduced by 12.7%, whereas the RMS driving torque of the optimized tri-wheel tail mechanism was reduced by 17.6%. Therefore, the results of robust optimal design using the simulations performed in this study can be considered reliable because the reduction in driving torque in both the simulation and actual experiment exhibits similar numerical values and trends.

# 5 Conclusion

In this study, a robust optimal design of a tri-wheel tail mechanism for a stair-climbing robot was performed to obtain performance improvements for stairs of various sizes and different climbing speeds as user conditions. The objective function was to minimize the minimum required friction coefficient for a mobile robot to climb stairs without slipping. The tri-wheel tail mechanism was optimized through the design of simulations of the tri-wheel tail mechanisms with orthogonal arrays using a commercial dynamic simulation software tool. By applying the optimized tri-wheel tail mechanism, it was found that the minimum required friction coefficient significantly decreased compared to the model without the tri-wheel tail mechanism for stairs of various sizes and different climbing speeds. The performance

improvements were verified by measuring the driving torque during experiments using a prototype of the tri-wheel tail mechanism.

## Declarations

**Competing Interests** The authors declare that they have no conflict of interest.

## References

1. Hutter, M., Gehring, C., Jud, D., Lauber, A., Bellicoso, C.D., Tsounis, V., Hwangbo, J., Bodie, K., Fankhauser, P., & Bloesch, M. et al. (2016). Anymal-a highly mobile and dynamic quadrupedal robot. In *2016 IEEE/RSJ International Conference on Intelligent Robots and Systems* (IROS) (pp. 38–44). IEEE
2. Choi, D., Kim, J.R., Cho, S., Jung, S., & Kim, J. (2012). Rocker-pillar: Design of the rough terrain mobile robot platform with caterpillar tracks and rocker bogie mechanism. In *2012 IEEE/RSJ International Conference on Intelligent Robots and Systems* (pp. 3405–3410). IEEE
3. Kim, H., Kim, D., Yang, H., Lee, K., Seo, K., Chang, D., & Kim, J. (2008). Development of a wall-climbing robot using a tracked wheel mechanism. *Journal of Mechanical Science and Technology, 22*(8), 1490–1498.
4. Komura, H., Endo, G., & Suzumori, K. (2016) Eccentric crank rover: A novel crank wheel mechanism with eccentric wheels. In *2016 IEEE/RSJ International Conference on Intelligent Robots and Systems (IROS)* (pp. 1048–1053). IEEE
5. Kim, Y., Kim, J., Kim, H. S., & Seo, T. (2019). Curved-spoke tri-wheel mechanism for fast stair-climbing. *IEEE Access, 7*, 173766–173773.
6. Kim, Y., Lee, Y., Lee, S., Kim, J., Kim, H. S., & Seo, T. (2020). Step: A new mobile platform with 2-dof transformable wheels for service robots. *IEEE/ASME Transactions on Mechatronics, 25*(4), 1859–1868.
7. Moore, E., Campbell, D., Grimminger, F., & Buehler, M. (2002). Reliable stair climbing in the simple hexapod'rhex. *Proceedings 2002 IEEE International Conference on Robotics and Automation (Cat. No. 02CH37292), 3*, 2222–2227.
8. Campbell, D., & Buehler, M. (2003). Stair descent in the simple hexapod'rhex'. *2003 IEEE International Conference on Robotics and Automation (Cat. No. 03CH37422), 1*, 1380–1385.
9. Son, D., Shin, J., Kim, Y., & Seo, T. (2022). Levo: Mobile robotic platform using wheel-mode switching primitives. *International Journal of Precision Engineering and Manufacturing*, 1–10.
10. Shin, J., Son, D., Kim, Y., & Seo, T. (2022). Design exploration and comparative analysis of tail shape of tri-wheel-based stair-climbing robotic platform. *Scientific Reports, 12*(1), 19488.
11. Seo, T., Casarez, C.S., & Fearing, R.S. (2017). High-rate controlled turning with a pair of miniature legged robots. In *2017 IEEE International Conference on Robotics and Automation (ICRA)* (pp. 5962–5968). IEEE

12. Unver, O., Uneri, A., Aydemir, A., & Sitti, M. (2006). Geckobot: A gecko inspired climbing robot using elastomer adhesives. In *Proceedings 2006 IEEE International Conference on Robotics and Automation, 2006. ICRA 2006.* (pp. 2329–2335). IEEE

13. Jusufi, A., Goldman, D. I., Revzen, S., & Full, R. J. (2008). Active tails enhance arboreal acrobatics in geckos. *Proceedings of the National Academy of Sciences, 105*(11), 4215–4219.

14. Norberg, R.Å. (1986). Treecreeper climbing; mechanics, energetics, and structural adaptations. *Ornis Scandinavica*, 191–209.

15. Guarnieri, M., Debenest, P., Inoh, T., Takita, K., Masuda, H., Kurazume, R., Fukushima, E., & Hirose, S. (2009). Helios carrier: Tail-like mechanism and control algorithm for stable motion in unknown environments. In *2009 IEEE International Conference on Robotics and Automation* (pp. 1851–1856). IEEE

16. Seo, T., & Sitti, M. (2012). Tank-like module-based climbing robot using passive compliant joints. *IEEE/ASME Transactions on Mechatronics, 18*(1), 397–408.

17. Lee, G., Wu, G., Kim, S.H., Kim, J., & Seo, T. (2012). Combot: Compliant climbing robotic platform with transitioning capability and payload capacity. In *2012 IEEE International Conference on Robotics and Automation* (pp. 2737–2742). IEEE

18. Kacker, R. N., Lagergren, E. S., & Filliben, J. J. (1991). Taguchi's orthogonal arrays are classical designs of experiments. *Journal of Research of the National Institute of Standards and Technology, 96*(5), 577.

19. Rout, B., & Mittal, R. (2008). Parametric design optimization of 2-dof r-r planar manipulator–a design of experiment approach. *Robotics and Computer-Integrated Manufacturing, 24*(2), 239–248.

20. Lee, K., & Kim, J. (2000). Controller gain tuning of a simultaneous multi-axis pid control system using the taguchi method. *Control Engineering Practice, 8*(8), 949–958.

21. Peace, G.S. (1993). *Taguchi Methods: A Hands-on Approach*. Addison-Wesley.

22. Kim, D., Hong, H., Kim, H. S., & Kim, J. (2012). Optimal design and kinetic analysis of a stair-climbing mobile robot with rocker-bogie mechanism. *Mechanism and Machine Theory, 50*, 90–108.

23. Smith, L.M., Quinn, R.D., Johnson, K.A., & Tuck, W.R. (2015). The tri-wheel: A novel wheel-leg mobility concept. In *2015 IEEE/RSJ International Conference on Intelligent Robots and Systems (IROS)* (pp. 4146–4152). IEEE

24. RecurDyn, FunctionBay Inc. https://functionbay.com/en

25. Taguchi, G., Cariapa, V. (1993). *Taguchi on Robust Technology Development*.

26. Thueer, T., & Siegwart, R. (2010). Mobility evaluation of wheeled all-terrain robots. *Robotics and Autonomous Systems, 58*(5), 508–519.

27. Thüer, T. (2009). Mobility evaluation of wheeled all-terrain robots: Metrics and application. In *PhD thesis, ETH Zurich*

28. Siegwart, R., Lamon, P., Estier, T., Lauria, M., & Piguet, R. (2002). Innovative design for wheeled locomotion in rough terrain. *Robotics and Autonomous Systems, 40*(2–3), 151–162.

29. Lee, Y., Lee, S., Oh, J., Kim, H. S., & Seo, T. (2019). Optimal design of shape of a curved tri-wheel mechanism for various sizes of stairs. *Journal of Institute of Control, Robotics and Systems, 25*(11), 1014–1020.

**JeongPil Shin** received his B.S degree in Mechanical Engineering from Hanyang University in 2020. He is currently working toward his M.S. degree in Mechanical Engineering at Hanyang University. His research interests lie in the design of robot mechanisms.

**YoungHwan Kim** received his B.S. degree in Mechanical Engineering from Hanyang University in 2022. He is currently working toward his M.S. degree in Mechanical Engineering at Hanyang University. His research interests lie in the design of robot mechanisms.

**Dong-Yoon Kim** received his B.S. degree in Mechanical Engineering from Jeonbuk National University, Korea, in 2020. He is currently pursuing an integrated Ph.D. in Mechanical Engineering, Hanyang University, Korea. His research interests include abnormality detection, nonlinear transformation, deep learning, vibration attenuation, and penetration analyses.

**Gil Ho Yoon** received his B.S. degree in Mechanical and Aerospace Engineering from Seoul National University in 1998, and he received his M.S. and Ph.D. degrees in Mechanical and Aerospace Engineering from Seoul National University in 2000 and 2004, respectively. Dr. Yoon is currently a Professor at School of Mechanical Engineering, Hanyang University, Korea. His research interests include topology optimization, model order reduction, multiphysics system design, acoustic/vibration absorption analysis, and penetration analysis.

**TaeWon Seo** received B.S. and Ph.D. degrees from the School of Mechanical and Aerospace Engineering, Seoul Nat'l Univ., Korea in 2003 and 2008, respectively. He is a professor at the School of Mechanical Engineering, Hanyang University, South Korea. Before Hanyang University, he was a postdoctoral researcher at Nanorobotics Laboratory, Carnegie Mellon University, a visiting professor at Biomimetic Millisystems Lab., UC Berkeley, a visiting scholar at the University of Michigan, and an associate professor at the School of Mechanical Engineering, Yeungnam University, South Korea. His research interests include robot design, analysis, control, optimization, and planning. Dr. Seo received the Best Paper Award of IEEE/ASME Transaction on Mechatronics in 2014. He is a Technical/Associate Editor of IEEE/ASME Transaction on Mechatronics and Intelligent Service Robots and was an Associate Editor of IEEE Robotics and Automation Letters.